Chapter 5

Push-Pull Mechanism of Hydrodenitrogenation over Silica Supported MoP, WP, and MoS_2 Hydroprocessing Catalysts

5.1. Introduction

Silica supported molybdenum phosphide, MoP/SiO_2, and tungsten phosphide, WP/SiO_2, were employed to study the mechanism of liquid phase catalytic hydrodenitrogenation at 3.1 MPa using a series of pentylamines of different structures. Removal of nitrogen occurred primarily by an E2 elimination mechanism involving acidic and nucleophilic species on the surface in a push-pull process. Similar results were obtained with a reference MoS_2/SiO_2 sample tested at the same conditions. This indicated that sulfur was probably present on the active surface and assisted in the mechanism of HDN. The Mo and W phosphides, however, showed higher activity in quinoline HDN than the MoS_2/SiO_2, indicating that their surface composition was unique.

Transition metal phosphides have recently been reported to be active hydroprocessing catalysts, extending the range of known active compounds for this class of reactions. In particular MoP (1, 2), WP (3), Ni_2P, and Co_2P (4) have been shown to give high conversions in hydrodesulfurization (HDS) and especially hydrodenitrogenation (HDN) of model petroleum feedstocks. Little is known about the nature of these catalytic materials, and studies to elucidate their behavior are of practical and fundamental interest. We have undertaken the present investigation to assess the performance of MoP and WP

when deposited on a neutral support, and to understand the mechanism by which they carry out the HDN reaction.

Elucidation of the mechanism of HDN is complicated for several reasons. Not only is the reaction affected by the conditions at which it is run, such as hydrogen pressure, delivery rate, and the presence of H_2S, but also the catalyst may be complex and posses multiple functionalities, such as hydrogenation and hydrogenolysis sites (5). It is likely that the mechanism and rate of reaction will depend ultimately on the nature of its interaction with the reacting molecule. The classical mechanism of denitrogenation is the Hofmann degradation of amines (6), but there are a number of other possibilities (7, 8, 9) such as S_N1, E1, S_N2, E2, and metallacycle or metal alkyl formation pathways These pathways are displayed diagrammatically in Scheme 5.1. The mononuclear pathways (S_N1 and E1) start with the generation of a carbocation by quaternization of an amine followed by cleavage of ammonia. Nucleophilic substitution occurs by attack of a nucleophile (HS^-) on the carbonium ion (the original α-carbon), while elimination occurs by abstraction of a proton by the nucleophile (from the original β-carbon). The binuclear pathways (S_N2 and E2) begin with the formation of the quaternized ammonium compound as in the mononuclear case, but without scission of ammonia. Nucleophilic substitution occurs by attack of a nucleophile on the α-carbon while elimination (E2) occurs by attack on the β-carbon to abstract a proton and form an olefin. The pathways involving reactions with metals (metallacycle and metal alkyl formation) require activation of the α-carbon to the nitrogen (10). These pathways likely occur with metallic catalysts like Ir or Os, but are not preferred with the phosphide or sulfide catalysts considered here.

Scheme 5.1: Potential mechanisms of alkylamine HDN reactions.

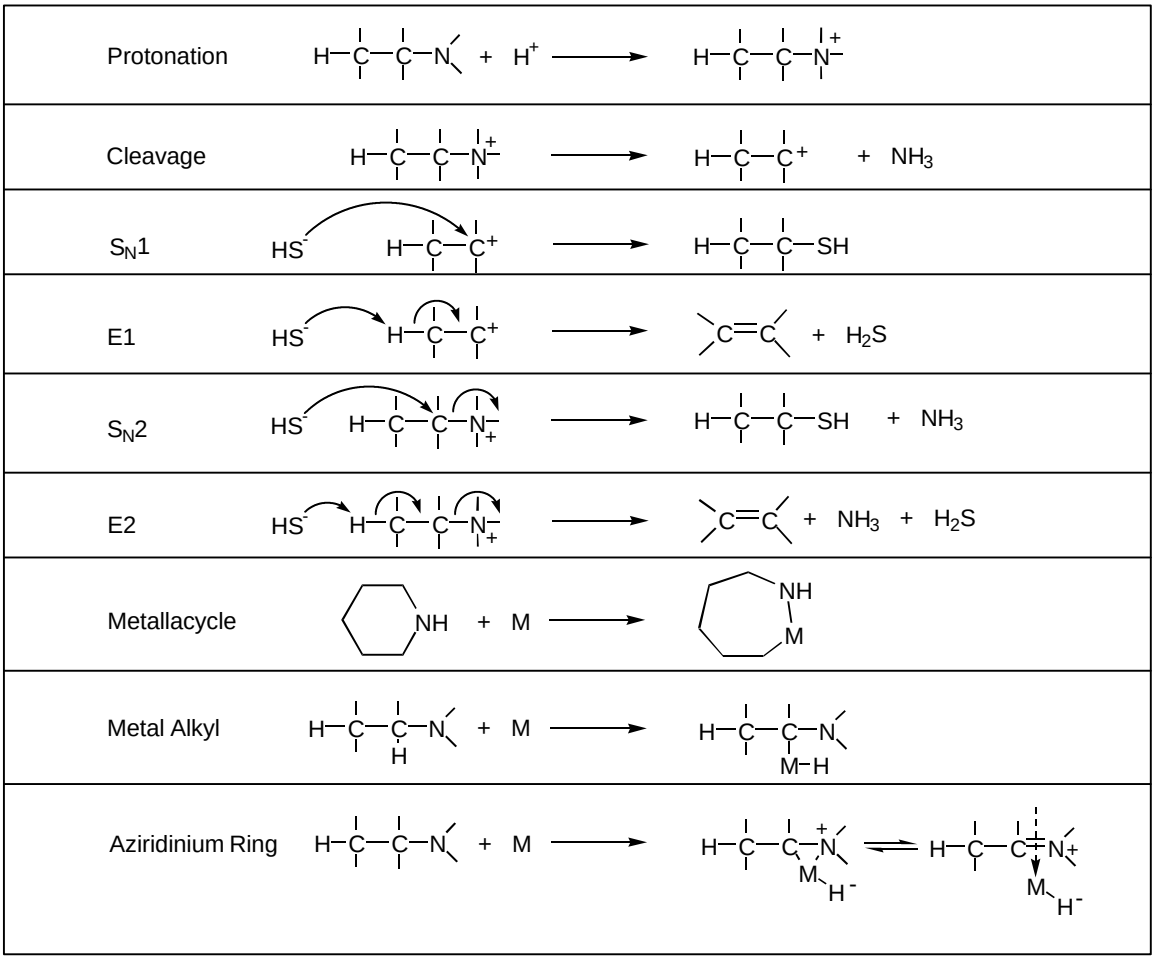

In order to ascertain the operative mechanism (S_N1, E1, S_N2, or E2) on the catalysts, use was made of the method of Breysse (7, 8, 9) employing a series of pentylamines of different structure. The original work was carried out in the vapor phase, and we have adapted the method to employ more realistic conditions of liquid phase and high pressure (3.1 MPa).

The catalysts employed in this study were supported on the neutral support silica in order to minimize the role of acid sites on the support. The use of silica for

hydroprocessing catalysts has not been widely studied because weak interactions with the active phase generally lead to low dispersions (11). However, it has been found that low loading (2 – 4 wt %) samples of MoS_2/SiO_2 can perform better than their Al_2O_3 counterparts (12, 13). In the present study, the low interactions expected with SiO_2 are ideal for studying the intrinsic properties of MoP and WP compared to MoS_2.

5.2. Experimental

Silica supported phosphides were prepared by incipient wetness impregnation with aqueous metal phosphate precursors, followed by controlled reduction in flowing hydrogen. The silica support (Cabot, Cabosil L90, 99.8%) consisted of 0.2 - 0.3 μm aggregates of spherical particles of ~30 nm diameter prepared by vapor phase hydrolysis of $SiCl_4$ in a $H_2 – O_2$ flame (14). Stoichiometric amounts of ammonium paramolybdate, $(NH_4)_6Mo_7O_{24}•4H_2O$ (Aldrich, 99%) or ammonium metatungstate $(NH_4)_6W_{12}O_{39}•xH_2O$ (Aldrich, 90%) were combined with ammonium phosphate $(NH_4)_2HPO_4$ (Aldrich, 99%) in distilled water, and the solution was used to impregnate the silica support. The moist paste was calcined in air at 773 K for 6 h, ground and mixed, then pressed, broken, and sieved between 650 and 1180 μm screens to form pelletized supported phosphate materials. These precursor phosphates were loaded in quartz glass u-tube reactors, and were reduced to phosphides using linear temperature ramps in flowing hydrogen. Hydrogen flow was set at 650 $\mu mol\ s^{-1}\ g^{-1}$ starting material (e.g. 300 cm^3(NTP) min^{-1} H_2 flow for a 0.300 g sample) for all syntheses. Species in the effluent were identified

periodically (2-5 s) by a mass spectrometer (Dycor/Ametek MA100) to follow the progress of the reaction. Water was the principle gaseous reaction product detected. Occasionally, small amounts of a yellow insoluble deposit were formed downstream in the reactor following higher temperature reactions of WP/SiO_2. After reduction, the phosphide was cooled to room temperature under 65 μmol s^{-1} helium and typically was passivated progressively by flowing 78 μmol s^{-1} 0.1 % O_2/He overnight, followed by 13 μmol s^{-1} of 0.5 % O_2/He for 2 h. The reactor was then disconnected from the flow system, and oxygen , carbon dioxide, and water from ambient air were allowed to diffuse in for 24 h before collecting the sample from the tube.

MoS_2/SiO_2 samples were prepared by sulfiding 5 % MoO_3/SiO_2 for 2 h in a stream of 10 % H_2S/H_2 at 678 K and a heating rate of 0.0833 K s^{-1} (5 K min^{-1}). The sulfide samples used for hydroprocessing were sulfided directly from the oxide within the catalytic reactor at a flow rate of 98 μmol s^{-1} (150 cm^3(NTP) min^{-1}) at atmospheric pressure. The characterization of the sulfide samples by O_2 chemisorption also directly followed sulfidation of the oxide. For the chemisorption measurements, 0.3 g of oxide were sulfided in 650 μmol $s^{-1}g^{-1}$ (300 cm^3 (NTP) min^{-1}) of 10 % H_2S/H_2 using the same temperature program noted for the catalyst samples.

All gases were supplied by Air Products. Hydrogen, helium, and carbon monoxide were all 99.999% pure, and were passed through a water trap (Alltech) before contacting the sample. Specialty mixtures, including 0.5 % O_2/He, 30 % N_2/He, and 10 % H_2S/H_2 were used as received.

The total dynamic CO and O_2 uptakes were measured by passing pulses of CO or O_2 (5.6 μmol) in a stream of 40 μmol s^{-1} helium over samples at room temperature.

Measurements performed on freshly reduced samples following cooling in helium are termed here *in situ* uptakes, while measurements on air exposed samples rereduced to 723 K for 2 h are denoted *ex situ*. The O_2 uptake was modified by a factor of 2 to account for dissociative adsorption on the surface. Surface area measurements were performed with a Micromeritics 2000 sorption unit.

X-ray diffraction (XRD) spectra were collected with a Scintag XDS-2000 X-ray diffractometer using Ni-filtered Cu K_α (λ = 0.1541 nm) radiation. Scans were collected at a rate of $0.035^o\ 2\theta\ s^{-1}$ and in increments of $0.03^o\ 2\theta$.

Two types of hydrotreating reactions were investigated. The first was to assess the activity of the catalysts, the second was used to study the mechanism of HDN. Activity was measured by hydrotreating of a model liquid containing quinoline and dibenzothiophene at 643 K (370 ^oC) and 3.1 MPa (450 psig) in an upward-flow, fixed-bed reactor as described in chapter 2. Compositional characteristics of the model feed liquid were summarized previously in Table 2.1. With the exception of tetradecane, which was purchased from Fisher (99%), chemicals were obtained from Aldrich, and had a purity level of 97+%.

The mechanism of HDN was studied by hydrodenitrogenation of solutions containing 2000 ppm N as *n*-pentylamine ($C_5H_{13}N$, Acros, 99%), *tert*-pentylamine (Acros, 98%), or *neo*-pentylamine (TCI) dissolved in tetradecane (Fisher, 99%). These reactions were were carried out at 3.1 MPa and as a function of temperature for each catalyst. The pentylamine feed solutions also contained 3000 wppm S as dimethyldisulfide ($C_2H_6S_2$, Aldrich, 99%), as well as 2000 wppm *n*-octane (C_8H_{18}, Aldrich, 99%) as an internal standard.

The basis set of catalytic reaction results used was the percent of reactant converted to a given product, counting all of the detected species as 100 %. Only the liquid phase products were analyzed. The carbon balances on the amine reactants and their products were typically 90 % ± 10 %. Gas-liquid equilibria were considered in the atmospheric pressure samples (after collection) to help account for the volatility of the C_5 hydrocarbons and amines (15). Small amount of light products were found in dry-ice temperature condensate from the hydrogen (vapor) effluent, but it was not possible to accurately quantify this material, as complications arose from carryover of the liquid phase solvent tetradecane in the gas stream. Thus the slightly low carbon balances can be explained as either due stripping of the light molecules in the gas phase, or from coke formation from nitrogen molecules, as noted in the literature (16).

The composition of hydroprocessing liquids was identified with a Hewlett Packard 5890A gas chromatograph (equipped with a CP Sil 5B column) on samples collected at 2-3 h intervals. Steady state was typically achieved after about 60 h of reaction time at a given condition. Reaction products were identified through matching of retention times with commercially available molecules, as well as by GC/MS analysis. The GC/MS combined a Fisons Carlo Erba 8060 series gas chromatograph, using a HP-5MS 5% phenylmethylsiloxane stationary phase, with a VG Quattro triple quadrupole mass spectrometer operated in the electron impact – positive ion mode.

To start a catalytic reaction, phosphide catalysts were pretreated in 100 μmol s^{-1} hydrogen at 723 K and 1 atm pressure for 2 h, while the sulfide catalyst was presulfided with a 10% H_2S/H_2 mixture at 678 K and 1 atm pressure for 2 h. After the pretreatment, the conditions were set to 3.1 MPa (450 psig), a hydrogen flow rate of 100 μmol s^{-1} (150

sccm), a liquid feed rate of 0.0833 cm^3 s^{-1} (5 cm^3 min^{-1}), and the desired temperature. For amine reactions, the amounts of catalysts used were 3.3 g of MoS_2/SiO_2, 1.4 g of MoP/SiO_2, and 3.1 g of WP/SiO_2. These amounts corresponded to roughly similar quantities (56, 70, and 58 μmol, respectively) of chemisorption sites. In the case of activity measurement for the MoS_2 reference, two experiments were conducted. In the first, the conditions were changed directly from amine HDN to model feed hydroprocessing, generating results similar to the blank. Thereafter, a new 5 % MoO_3/SiO_2 sample was prepared, characterized, and tested for hydroprocessing. This material had O_2 uptake equal to 27 μmol g^{-1}, and 2.59 g were loaded to the reactor, corresponding to 70 μmol of sites. For the SiO_2 blank, an arbitrary amount of 3 g was employed, as the material had negligible chemisorption of CO. Once started, the individual catalysts were used for extended sets of conditions (i.e. different molecules and temperatures). The duration of the total set of experiments was lengthy, requiring several months, but standard conditions were repeated periodically to verify that no deactivation occurred. Results from repeated conditions were similar, and were averaged to obtain the reported values.

5.3. Results and Discussion

5.3.1. Preparation and Characterization of Catalysts

Silica supported molybdenum phosphide, tungsten phosphide, and molybdenum sulfide catalysts were prepared by incipient wetness impregnation of silica support with

ammonium salts of Mo, W, and P dissolved in distilled water. Compositional characteristics of each sample are summarized in Table 5.1. The surface depositions of molybdenum and tungsten monophosphide were held constant at 1.156 mmol each of Mo, W, and P per gram of silica, leading to 12.8 wt% MoP/SiO_2 and 19.9 wt% WP/SiO_2, respectively. Sulfidation of a sample containing 5 wt% MoO_3 on SiO_2 led to 5.6 wt% MoS_2/SiO_2.

Table 5.1: Compositional characteristics of silica supported catalysts.

sample	wt%[†]	mmol metal g^{-1} SiO_2	metal atom nm^{-2} SiO_2
MoS_2/SiO_2	5.6	0.368	2.44
MoP/SiO_2	12.8	1.156	7.67
WP/SiO_2	19.9	1.156	7.67

[†] wt% MoP, WP, or MoS_2

Oxidic catalyst precursors were reduced to phosphide form by temperature-programmed reduction in hydrogen, and were subsequently passivated. Conditions used in the prereduction of samples from their respective phosphate precursor materials are summarized in Table 5.2. Prior to the reactivity measurements and *ex situ* CO uptake characterization, passivated phosphides were pretreated in hydrogen at 723 K for 2 h to remove the surface oxide layer.

Table 5.2: Preparation conditions of silica supported phosphides.

Sample	H_2 flow*	Heating rate K min^{-1}	Temperature max K	Soak time† h
MoP/SiO_2	650	5	850	2
WP/SiO_2	650	5	1000	2

* μmol H_2 g^{-1} oxide s^{-1}
† at maximum temperature

The temperature programmed reduction (TPR) trace at 5 K min^{-1} of MoP/SiO_2 is compared to that of bulk MoP in Figure 5.1. The predominant reduction features appeared at high temperatures, 680 K and 820 K for the supported sample, and 770 K and 920 K for the unsupported reference. The TPR traces of WP/SiO_2 and WP are shown in Figure 5.2. Again, the predominant reduction peaks occur at high temperatures, 890 K and 970 K for the supported material, and 1010 K for the unsupported reference.

X-ray diffraction patterns of the MoP/SiO_2 samples are shown in Figure 5.3. The patterns showed features of bulk MoP both before and after reaction. XRD patterns of the WP/SiO_2 samples are shown in Figure 5.4. Again, the patterns corresponded to those of bulk WP both before and after reaction in hydrotreating.

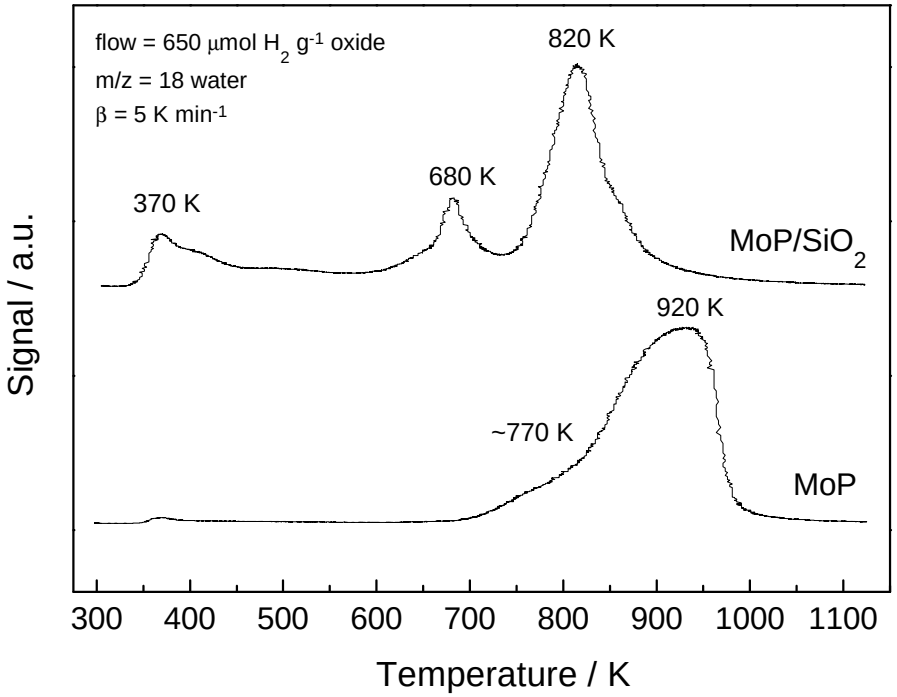

Figure 5.1: Temperature programmed reduction profiles in the preparation of MoP/SiO_2 and MoP at 0.0833 K s^{-1} (5 K min^{-1}).

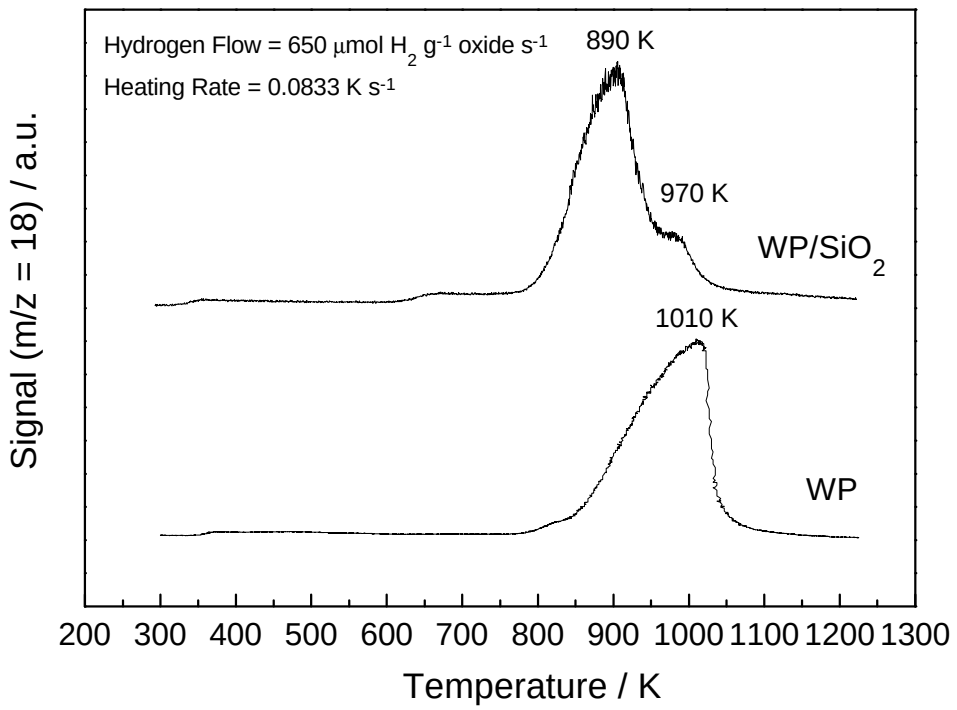

Figure 5.2: Temperature programmed reduction profiles in the preparation of WP/SiO_2 and WP at 0.0833 K s^{-1} (5 K min^{-1}).

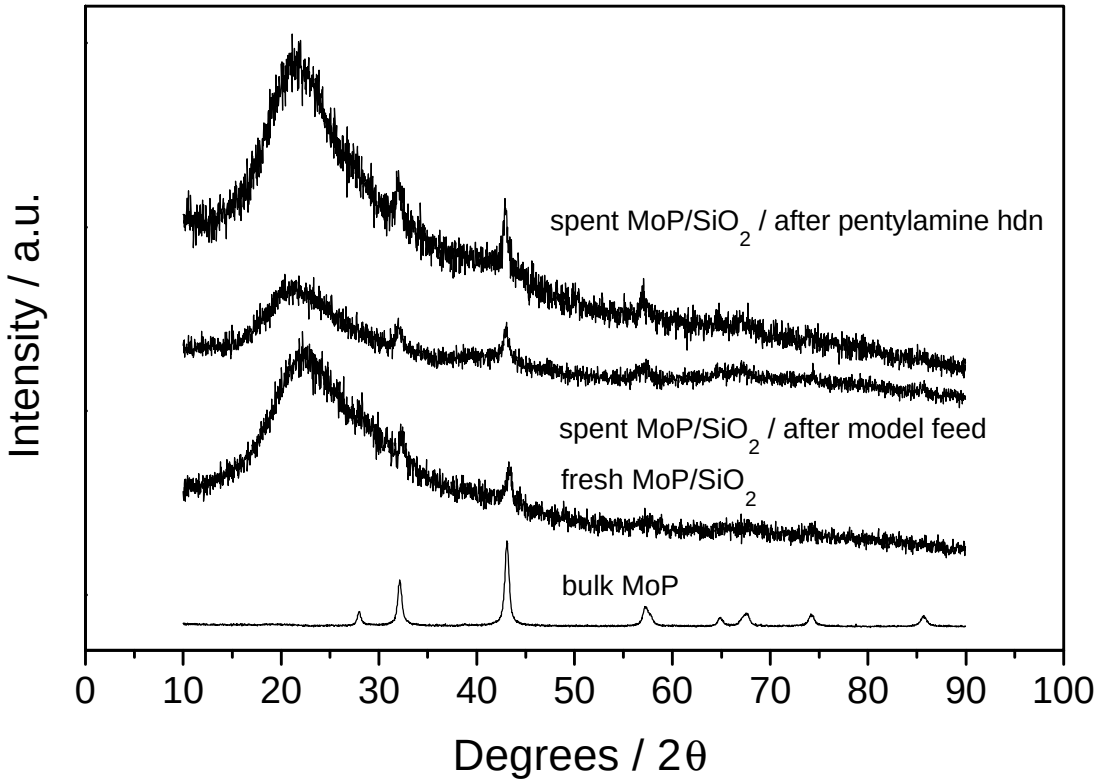

Figure 5.3: X-ray diffraction spectra for fresh and spent MoP/SiO_2 samples.

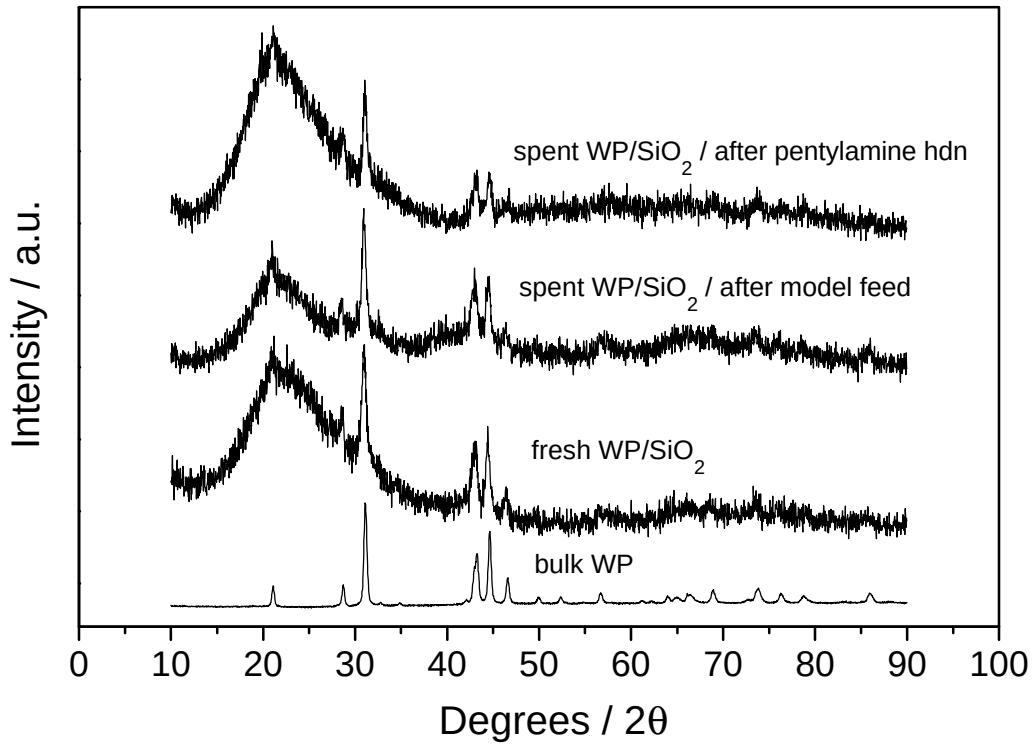

Figure 5.4: X-ray diffraction spectra for fresh and spent WP/SiO_2 samples.

The chemisorption and surface area properties of the catalysts are summarized in Table 5.3. The time course of the reaction in hydroprocessing dibenzothiophene and quinoline at 643 K and 3.1 MPa of MoP/SiO_2 and WP/SiO_2 are shown in Figure 5.5.

Table 5.3: Physical characteristics of silica supported catalysts.

Sample	Surface area[a] fresh	CO uptake[b] fresh	CO uptake[b] spent hdt[c]	CO uptake[b] spent amine[d]	Dispersion[e]
SiO_2 blank	91	0	0	0	-
MoS_2/SiO_2	93[f]	18(27)[g]	-	-	4.7(7.0)
MoP/SiO_2	50	50	26	26	3.8
WP/SiO_2	62	19	6.5	10.8	1.4

[a] $m^2\ g^{-1}$ catalyst; passivated catalysts; degassed in vacuum at 273 K for 24 h
[b] CO uptake at 298K in μmol g^{-1}; sample pretreated at 723 K in H_2
[c] following hydroprocessing of model feedstock
[d] following hydrodenitrogenation of pentylamines
[e] number of sites g^{-1} / number of moles of metal g^{-1} * 100%
[f] as oxide: MoO_3/SiO_2
[g] O_2 uptake at 78 K; sample presulfided at 678 K in 10% H_2S/H_2
(Value in parentheses is for second sample)

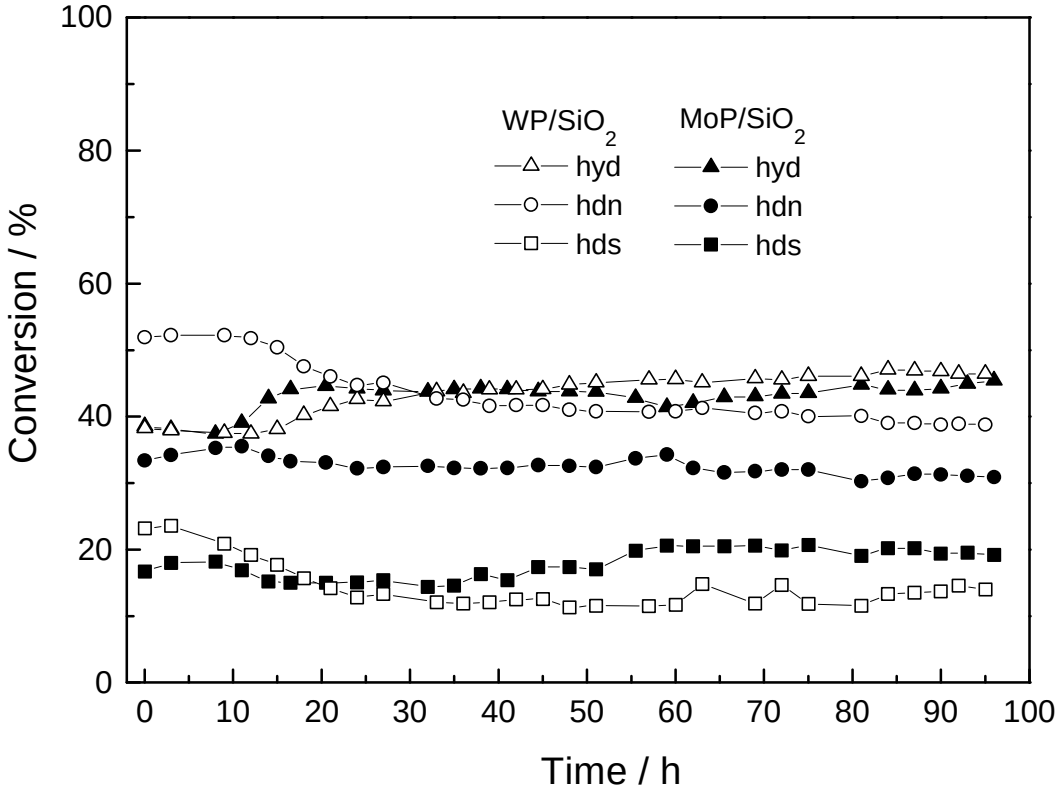

Figure 5.5: Time dependence of hydroprocessing reactivity of MoP/SiO_2 and WP/SiO_2 catalysts in the conversion of a model feed at 643 K and 3.1 MPa.

5.3.2. Pentylamine study

A study of the reactivity of a series of pentylamines was carried out to explore the effect of amine structure on the HDN reaction. The results for each individual amine are presented below.

5.3.2.1. *n*-Pentylamine

The product distributions for *n*-pentylamine HDN on silica supported MoP, WP, and MoS_2 are presented in Figure 5.6. The species favored at the lowest temperature in each case was dipentylamine. As temperature increased, pentane appeared along with small amounts of pentenes, pentanethiol, and tripentylamine. Total *n*-pentylamine conversions at all temperatures except 513 K increased in the order $MoP/SiO_2 < MoS_2/SiO_2 < WP/SiO_2$, however, the production of hydrocarbons increased in the order $MoP/SiO_2 < WP/SiO_2 < MoS_2/SiO_2$. The MoP/SiO_2 catalyst was the least active by both measures. Comparatively, the WP/SiO_2 had a higher propensity for condensation than MoS_2/SiO_2, while the MoS_2/SiO_2 had better hydrocarbon production.

The amounts and distributions of olefins at 533 K are summarized in Table 5.4, along with equilibrium concentrations estimated by thermodynamic calculations for this temperature. The predominant olefin formed on all catalysts was 1-pentene. Cis and trans 2-pentenes were observed for the WP/SiO_2 and MoS_2/SiO_2 catalysts at higher temperatures (513 K). In no cases were iso-pentene isomers observed.

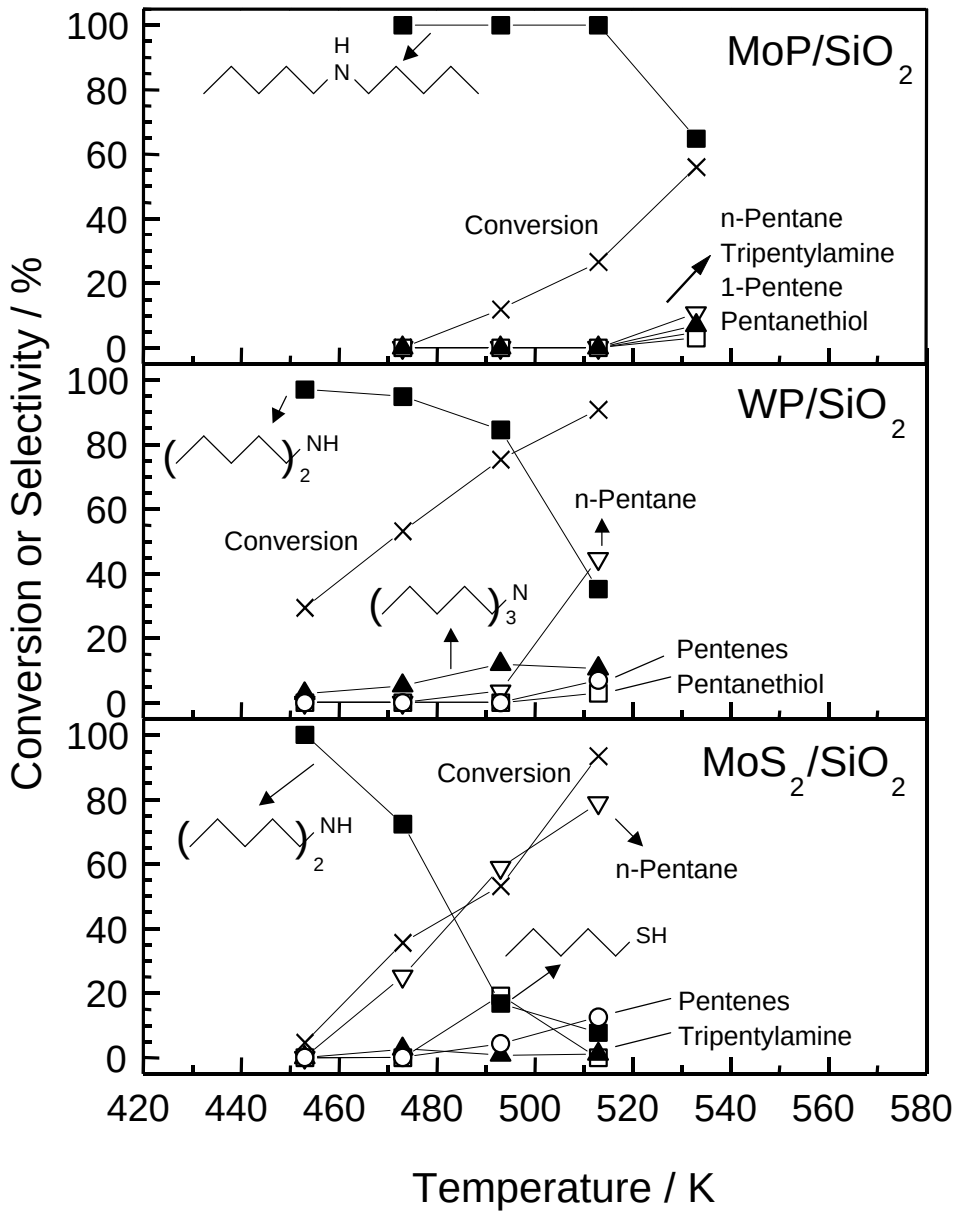

Figure 5.6: Product distribution in the hydrogenolysis of *n*-pentylamine on MoP/SiO_2, WP/SiO_2, and MoS_2/SiO_2 catalysts. × = Conversion, ■ = Dipentylamine, ∇ = *n*-Pentane, = Tripentylamine, O = Pentenes, □ = Pentanethiol.

Table 5.4: Olefin production and distribution for *n*-pentylamine HDN at 513 K

Sample	Total Olefins %	1-Pentene % selectivity	trans-2-Pentene % selectivity	cis-2-Pentene % selectivity
MoP/SiO_2 *	3	100	0	0
WP/SiO_2	6	42	30	28
MoS_2/SiO_2	12	39	39	22
equilibrium		7	69	24

% = % of *n*-pentylamine converted to olefins
% selectivity = % of total olefin as olefin i
* note that MoP results are from 533K. Total hydrocarbons for MoP at 513 K = 0.

Overall, the hydrocarbon distribution was consistent with the occurrence of an elimination reaction followed by dehydrogenation. However, significant amounts of pentanethiol were also found at 493 K on the MoS_2/SiO_2 catalyst, demonstrating the presence of N-S exchange as well.

5.3.2.2. *tert*-Pentylamine

The product distributions for *n*-pentylamine HDN on silica supported MoP, WP, and MoS_2 are presented in Figure 5.7. Hydrocarbons are the only products of tert-pentylamine HDN, with olefins being preferred at lower temperatures, and the alkane 2-methylbutane becoming more important at higher temperatures. The order of activity of the catalysts increased as $MoP/SiO_2 < WP/SiO_2 < MoS_2/SiO_2$, with the MoP catalyst being significantly less active than either the WP or MoS_2 catalysts. The relative amount of 2-methyl-2-butene was always greater than 2-methyl-1-butene on each catalyst.

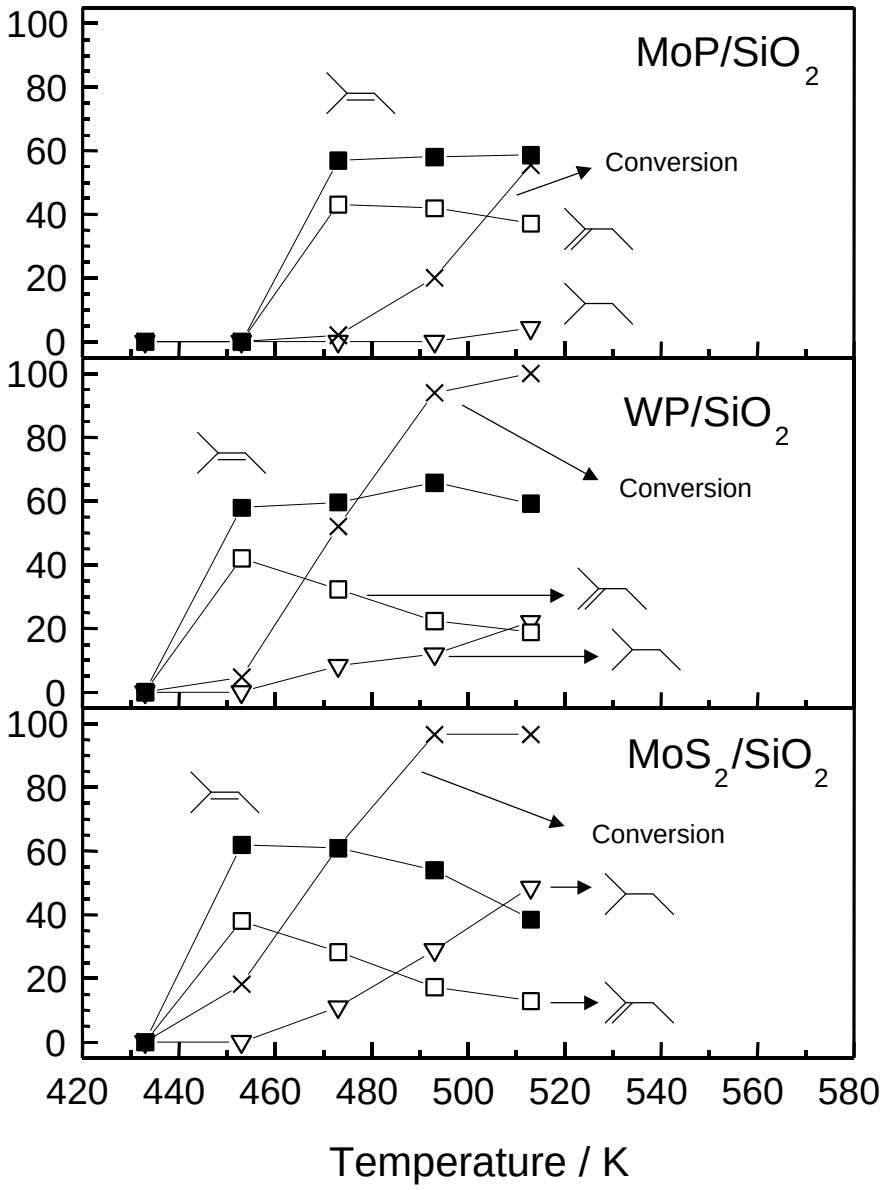

Figure 5.7: Product distribution in the hydrogenolysis of *tert*-pentylamine on MoP/SiO_2, WP/SiO_2, and MoS_2/SiO_2 catalysts. × = Conversion, ■ = 2-Methyl-2-butene, □ = 2-Methyl-1-butene, ∇ = *n*-Pentane.

Di(*tert*-pentyl)amine was not observed, in agreement with previous results (7), and its absence is attributed to steric effects.

5.3.2.3. *neo*-Pentylamine

The product distributions for *n*eo-pentylamine HDN on silica supported MoP, WP, and MoS_2 are presented in Figure 5.8. The initial product formed at low temperatures/conversions was di(*neo*-pentyl)amine. This molecule was the only product detected on the MoP catalyst. On WP and MoS_2, 2,2-dimethylpropane was observed at higher temperatures and was the only hydrocarbon product detected. The order of reactivity of the catalysts in terms of both total conversion and the formation of hydrocarbons increased in the order $MoP/SiO_2 < WP/SiO_2 < MoS_2/SiO_2$. Small amounts of nitrile were detected in products produced by WP and MoS_2 containing catalysts. Thus, *neo*-pentylamine is the only molecule for which a nitrile product was observed in this study.

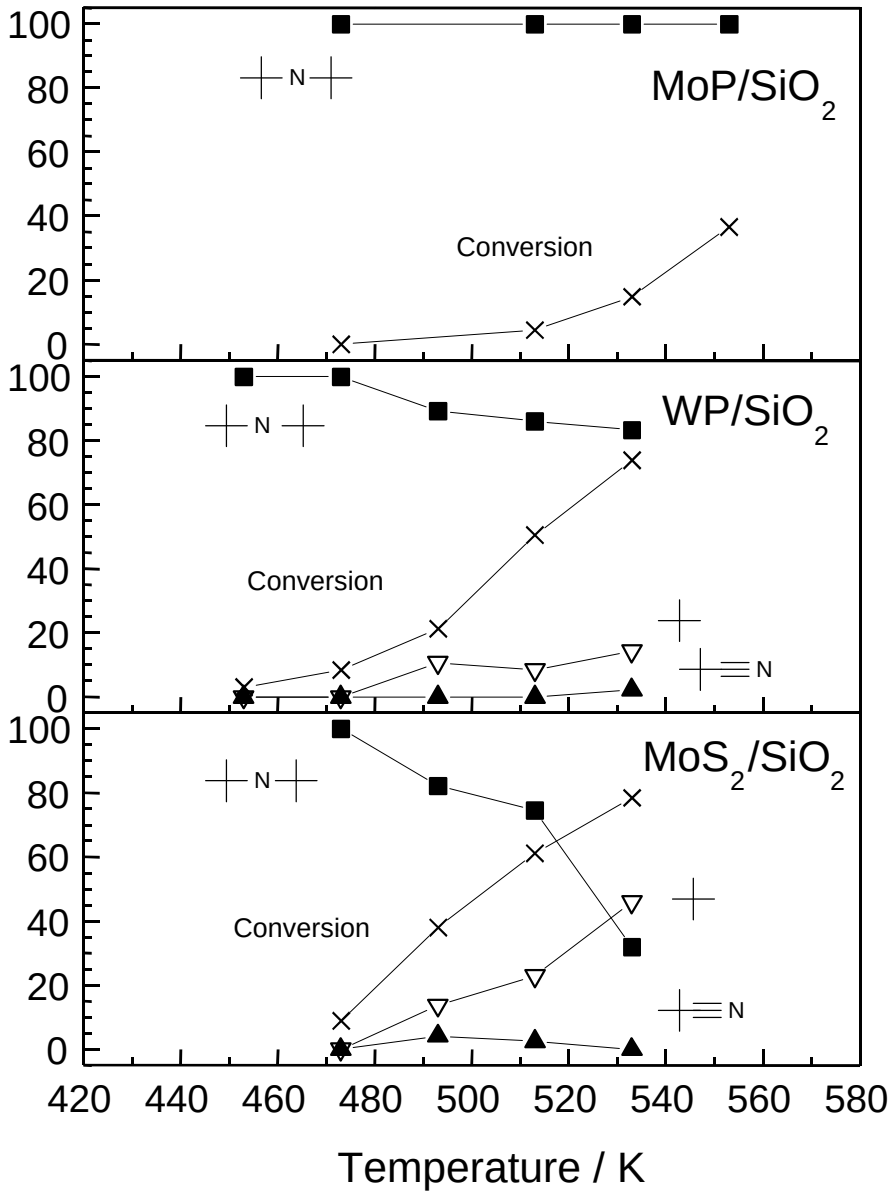

Figure 5.8: Product distribution in the hydrogenolysis of *neo*-pentylamine on MoP/SiO_2, WP/SiO_2, and MoS_2/SiO_2 catalysts. × = Conversion, ■ = Di(*neo*-pentyl)amine, ∇ = Dimethylpropane, = 2,2-Dimethylpropylnitrile.

5.4. Discussion

5.4.1. Preparation of silica supported phosphides

The preparative reduction profile for the MoP/SiO_2 catalyst is presented in Figure 5.1, and is compared to the reduction profile of bulk MoP taken under similar conditions. The reduction trace of MoP/SiO_2 shows a feature at low temperature (370 K) and two peaks at high temperature (680 K and 820 K). The low temperature feature is due to the dehydration of the sample, while the high temperature peaks are indicative of the reduction stages of the phosphate. The TPR trace of MoP/SiO_2 resembles that of MoP at lower heating rates, with the first peak producing no crystalline phase, and the second peak forming MoP. It can be seen that the synthesis reaction is substantially over at 850 K and this was used as the final reduction temperature for the preparation of the MoP/SiO_2 catalyst. A holding time of 2 h was used at this temperature to ensure completion of the reduction.

The bulk MoP reduction profile also shows these two high temperature reduction processes. However, because of the higher metal oxide content (the hydrogen flow rate was based on the weight of starting material), the first peak is unresolved and both peaks are shifted to higher temperature (770 K and 920 K). This is likely due to inhibition of the reduction process by the gas phase water vapor generated by reduction and the presence of larger particles (17).

The XRD spectra of the bulk MoP and supported MoP samples prepared at 850 K, before and after the hydrotreating reactions, are shown in Figure 5.3. The bulk MoP has

a pattern which corresponds exactly to that reported in the literature (powder diffraction file 24-771). MoP has a hexagonal WC type structure (strukturbericht designation B_h) with space group $P_{\bar{6}m2}$ and lattice parameters a_o = 322 pm and c_o = 319 pm (18). The supported MoP/SiO_2 shows a broad feature at ~22° 2θ produced by the amorphous silica support, and several distinct peaks which match those of the bulk MoP phase.

The preparative reduction profile for the WP/SiO_2 catalyst is presented in Figure 5.2, and is compared to the reduction profile for bulk WP taken under similar conditions. The reduction trace of WP/SiO_2 shows a slight feature at 370 K, a slight rise at 630 K, and a large peak at 890 K with a high temperature shoulder at 970 K. The feature at 370 K is due to dehydration of the sample, while the high temperature peaks are due to formation of phosphide. The slight rise at low temperature may be due small quantities of highly dispersed species, while the shoulder at high temperature may be due to small quantities of larger particles which reduce more like the bulk WP. It is clear from the figure that the reduction process is essentially completed at 1000 K, which was used as the maximum temperature in the preparation of WP catalyst. Again, a hold time of 2 h was used to ensure complete reduction of the sample.

The reduction profile of the bulk WP also shows the slight dehydration feature at 370 K, and a high temperature reduction peak at 1010 K. Again, the largest peak is shifted to higher temperature, likely as a result of inhibitive action of water vapor and the presence of larger particles in the bulk material. The assymetry in the shapes of the MoP and WP reduction profiles are due to the use of relatively high heating rates. This asymmetry disappears at lower heating rates (3).

The XRD spectra of the bulk WP and supported WP samples prepared at 1000 K, before and after hydrotreating reactions, are shown in Figure 5.4. The bulk WP has a pattern corresponding exactly to that reported in the literature (powder diffraction file 29-1364). WP adopts the orthorhombic MnP type structure (strukturbericht designation B31) with space group P_{nma} and lattice parameters a_o = 571 pm, b_o = 325 pm, and c_o = 623 pm (19). The supported WP/SiO_2 shows a broad feature at ~22° 2θ of the silica support, and several distinct peaks which match those of the WP phase.

The *ex situ* chemisorption characteristics and BET surface areas of samples reduced according to the specifications in Table 5.2, are summarized in Table 5.3. The surface area of the MoS_2/SiO_2 catalyst (93 m^2 g^{-1}) precursor was close to that of the support (91 m^2 g^{-1}) as its loading was low. The surface areas of the MoP/SiO_2 (50 m^2 g^{-1}) and WP/SiO_2 (62 m^2 g^{-1}) samples were significantly decreased from that of the support, a common finding for phosphorus promoted, supported catalysts (20, 21, 22). This is presumably an effect of pore blocking by phosphorus compounds. The use of elevated temperatures during sample reduction, 850 K for MoP/SiO_2 and 1000 K for WP/SiO_2, may also have contributed to the decrease in surface area by sintering the silica support. Chemisorption quantities of O_2 and CO for the fresh catalysts were moderate and were found to decrease somewhat after reaction for the phosphides. Measurements taken after reaction were carried out on recovered samples washed in hexane and rereduced at 723 K for 2 h. The CO uptakes of MoP/SiO_2 and WP/SiO_2 and O_2 uptake of MoS_2/SiO_2 were used to calculate dispersions based on stoichiometries for adsorption of 1 CO molecule and 1 O atom per surface metal atom. The dispersions are reported in Table 5.3. They

were low, 4.9 % for MoS_2/SiO_2, 4.3 % for MoP/SiO_2, and 1.6 % for WP/SiO_2, consistent with the observation of crystalline phases visible in the XRD patterns of the phosphides.

5.4.2. Reactivity in Hydroprocessing

The activity of the catalysts in the HDS of dibenzothiophene and the HDN of quinoline was evaluated in a three phase flow reactor at 643 K and 3.1 MPa. Figure 5.5 shows the conversions as a function of time on the silica supported MoP and WP in HDS and HDN. Both materials demonstrated good stability in their activity levels. It should be noted that those results were obtained with 58 μmol of sites of WP/SiO_2 and 70 μmol of sites of MoP/SiO_2 loaded in the reactor. The conversions were corrected to an equal sites basis, for WP/SiO_2, WP, and MoP, according to a first order kinetic expression as follows. Denoting X_1 as the conversion corresponding to a quantity of sites S_1, and X_2 as the conversion corresponding to S_2 sites, then the quantities are related by:

$$\ln(1 - X_2) = \left(\frac{S_2}{S_1}\right) * \ln(1 - X_1)$$

The corrected results for the supported MoP/SiO_2, WP/SiO_2, and MoS_2/SiO_2 are summarized in Table 5.5, along with results from bulk MoP and WP and the silica support. The MoP/SiO_2 catalyst was similar to the bulk MoP (1), while the WP/SiO_2 sample differed from its unsupported counterpart (3) having lower HDS activity and higher HDN hydrogenation. Importantly, note that hydroprocessing on MoS_2/SiO_2 was carried out on a separate, freshly prepared, sample from that used for the amines. The MoS_2/SiO_2 sample used for the amine study yielded results for the hydroprocessing of

quinoline and dibenzothiophene similar to the blank, when the conditions were switched directly from amine hdn to quinoline hdn.

Table 5.5: Quinoline hydrodenitrogenation, quinoline hydrogenation, and dibenzothiophene hydrodesulfurization as % conversion, for silica supported catalysts[a] during hydroprocessing of model feedstock at 643 K and 3.1 MPa.

Sample	% HDN	% HYD[b]	%HDS
SiO_2	2	32	1
MoS_2/SiO_2	11	45	31
MoP/SiO_2	31	45	20
WP/SiO_2[c]	46	46	16
MoP[c]	54	34	24
WP[c]	88	33	92

[a] Loading equals 70 μmol of sites for supported samples except WP/SiO_2 (58 μmol), or 30 m^2 for bulk samples.

[b] % HYD = Hydrogenation of quinoline to N-containing products.

[c] Value adjusted according to first order equation given in text.

5.4.3. Study of the Mechanism of HDN

It is well accepted that HDN is more difficult than HDS in hydroprocessing because of the higher strength of C-N bonds by 3-9 kcal mol^{-1} versus C-S bonds (23). The high activity of the phosphide catalysts for HDN was unusual and prompted investigation of the mechanism of HDN. A method described by the group of Breysse (7, 8, 9) utilizing a series of pentylamines of different structure was adapted to high-pressure, liquid-phase

conditions in our study. The amines consisted of *n*-pentylamine, *tert*-pentylamine, and *neo*-pentylamine and their structure and properties are described in Table 5.6.

The expected relative reactivities of the pentylamines are summarized in Table 5.7, as described by Cattenot *et al*. (7). *neo*-Pentylamine contains no β-hydrogen atoms and is sterically hindered, so is expected to be the least reactive molecule in the series. *tert*-Pentylamine has the greatest number of β-hydrogen atoms, and forms the most stable carbocation counterpart, so it is the most reactive molecule in the series. *n*-Pentylamine has an intermediate number of β-hydrogen atoms, is the least sterically hindered, and is expected to have intermediate activity. Carbocations of *neo*-pentylamine and *n*-pentylamine are expected to have similar stability.

The conversions to hydrocarbons of each catalyst for each of the three amines are plotted in Figure 5.9. The trend for the three pentylamine HDN reactions over MoP/SiO_2, WP/ SiO_2, and MoS_2/SiO_2 catalysts is for increased reactivity from *neo* < *n* < *tert*. Overall, this order is consistent with C-N bond scission occurring primarily by an E2 mechanism on all three catalysts (Table 5.7).

Temperature programmed desorption studies show that this species decomposes to release ammonia and ethylene in equal proportions, but in a nonconcerted manner. A possible sequence of steps for the transformation is depicted in Scheme 5.2.

Table 5.6: Relative properties of pentylamines for HDN reaction

Reactant	Structure	# α-Hydrogen	# β-Hydrogen	steric hindrance	carbocation stability	carbanion stability
n-Pentylamine	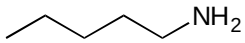	2	2	low	low	high
tert-Pentylamine	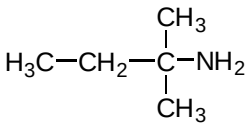	0	8	high	high	low
neo-Pentylamine	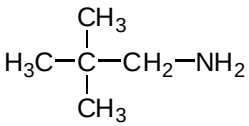	2	0	med	med	med

Table 5.7 : Relative reactivities of pentylamines according to possible reaction mechanisms.

Reactant	# β-Hydrogen	S_N1	S_N2	E1	E2
n-Pentylamine	2	very low	high	very low	medium high
tert-Pentylamine	8	high	very low	very high	high
neo-Pentylamine	0	very low	very low	none	none

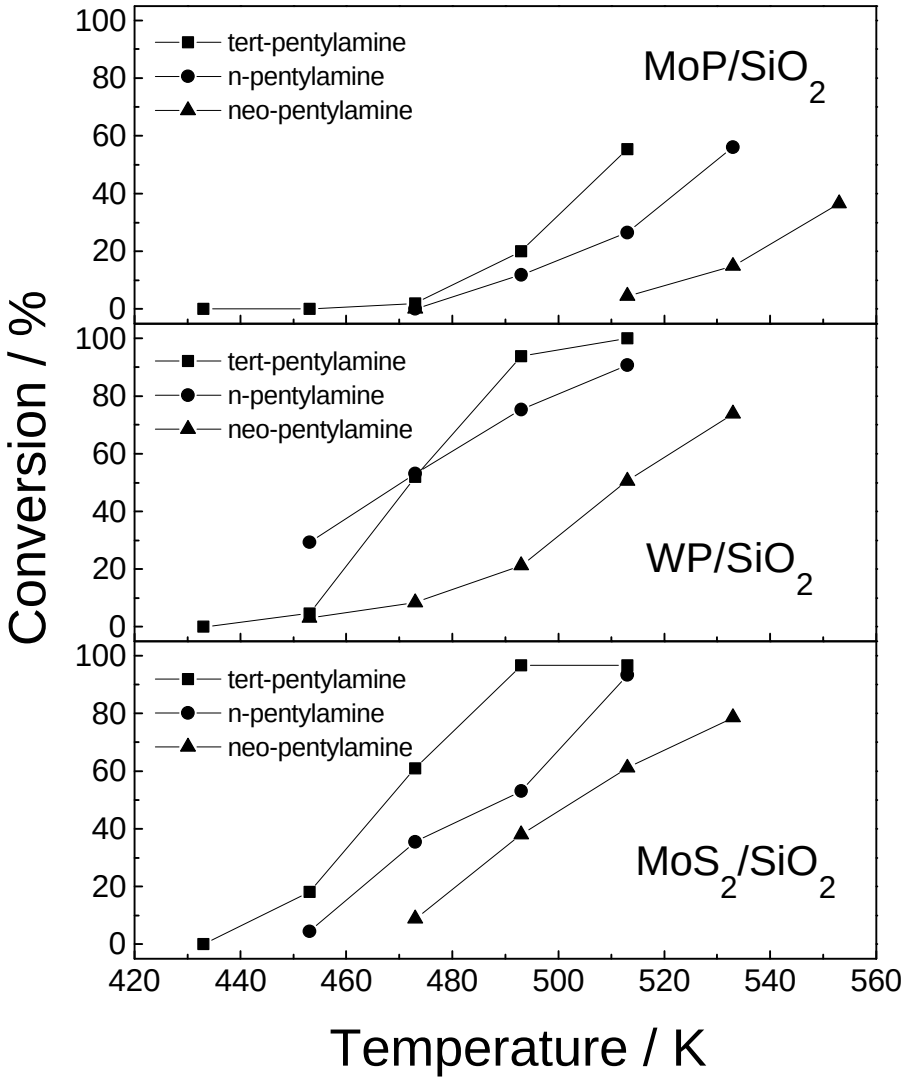

Figure 5.9: Total conversion of pentylamines over MoP/SiO_2, WP/SiO_2, and MoS_2/SiO_2 catalysts.

Scheme 5.2: Push - pull mechanism in the HDN of an alkylamine.

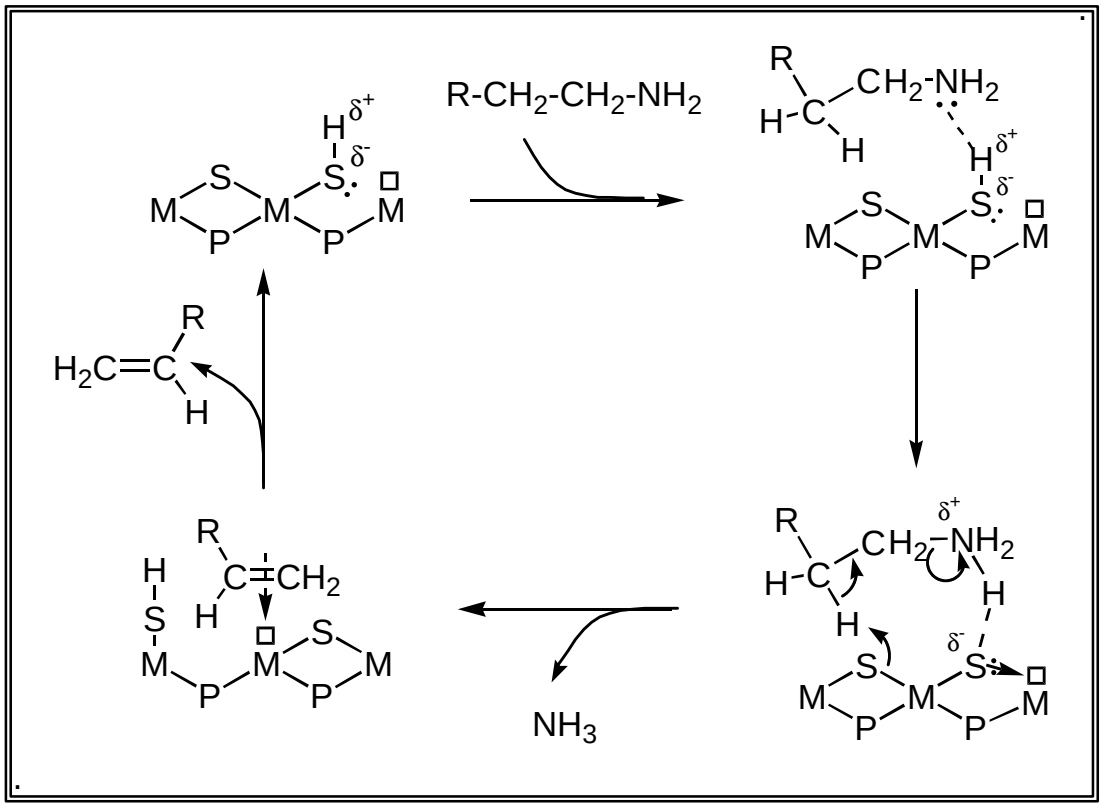

In this scheme we have taken the surface of the phosphide catalyst to be populated with sulfur species which provide Br□sted acidity in the form of sulfhydril groups, as well as nucleophilic centers. The exact structure of these groups is uncertain, and the forms shown in Scheme 5.2 should be considered illustrative, as other possibilities exist. However, the main features of the mechanism are otherwise consistent with the known observations. The amine first interacts with a Br□sted site on the surface to adsorb as an alkylammonium species. This then undergoes a β-hydride elimination by attack by a surface nucleophilic center. This is exactly an E2 elimination (Scheme 5.1) with the role of the surface now explicitly indicated, and results in the release of ammonia, as found in

the TPD experiments. The olefin interacts with the coordinatively unsaturated site on the surface to be released in a subsequent step.

The reactivity patterns of *n*-pentylamine and *tert*-pentylamine are consistent with the above mechanisms. In particular, for *n*-pentylamine it is likely that 1-pentene was the primary reaction product as it was the major olefin product formed at low temperatures (Figure 5.6, Table 5.4). At higher conversions the 1-pentene intermediate was hydrogenated to form *n*-pentane or isomerized by double bond migration to form *cis* and *trans* 2-pentenes. Importantly, no *iso*-pentenes were observed, indicating that carbonium ion intermediates such as those formed by S_N1 or E1 pathways were not formed. The lack of skeletal isomerization of the hydrocarbon suggests that the double bond migration step also occurred by a push-pull type mechanism, as proposed in Scheme 5.3.

Again, in Scheme 5.3 the surface structures are pictorial representations. Thermodynamic calculations show that 2-pentene is favored over 1-pentene, and *trans*-2-pentene is favored over *cis*-2-pentene. In the case of *n*-pentylamine the cis-trans distribution in the catalyst effluent was skewed toward 1:1 suggesting a kinetic control over the double bond migration step.

In the case of *tert*-pentylamine, the products of reaction were exclusively olefins and paraffins. The formation of 2-methyl-2-butene was preferred over 2-methyl-1-butene over each catalyst. This result shows preference for the thermodynamically favored triply substituted olefin product compared to the kinetically favored product having 3 times more available β-hydrogen atoms (6:2) for E2 elimination. Since E1 elimination is unlikely (as concluded earlier), this suggests that the pentenes can isomerize readily.

Scheme 5.3: Push - pull mechanism in the isomerization of an olefin.

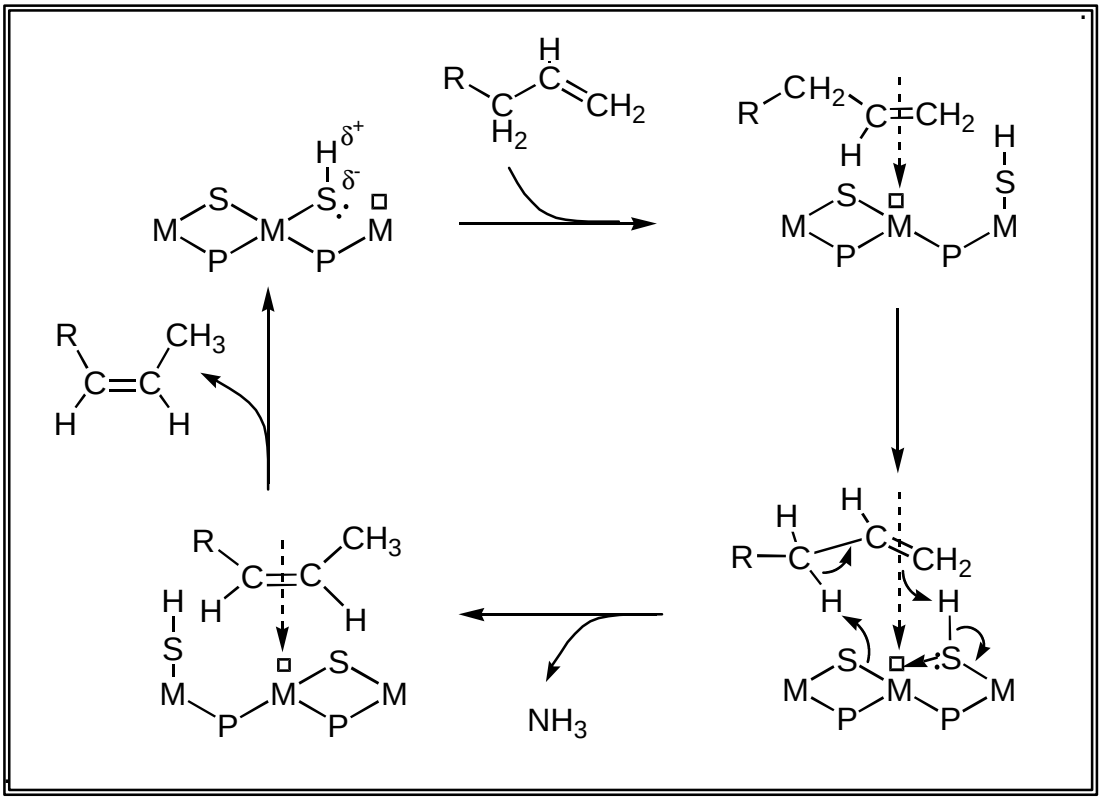

The reactions of *neo*-pentylamine fall in a different category from those of *n*-pentylamine and *tert*-pentylamine because the molecule doesn't have any β-hydrogen, making standard E1 and E2 elimination reactions impossible. Similarly, there is no γ-elimination as indicated by the absence of methylbutenes (24). As far as nucleophilic substitutions are concerned, the S_N1 route is unlikely because the intermediary primary carbonium ion is unstable, while the S_N2 pathway is partially blocked by steric hindrance. There is a possibility of hydride attack to displace the amine group, as the existence of hydride species associated with metal centers has been suggested before (25), as charged

species in spillover on neutral silica support (26), and organometallic HDN reactions involving lithium aluminum hydride (27). However, again this route appears unlikely because the hydride is likely to be held strongly. Finally, a homolytic reaction pathway can be considered involving H radicals (28, 29). This probably does not occur because of the lack of skeletal isomerization and β-scission products.

The more likely scenario in the case of *neo*-pentylamine is activation of an alpha carbon by one of the metal-centered reactions noted in Scheme 5.1. This would be followed by a series of hydrogenation and reductive elimination steps to produce the neo-pentane or the 2,2-dimethylpropylnitrile species. Nitriles have been reported before in the reactions of primary amines, nitrile formation being favored by lower pressures (30), and the absence of hydrogen (31, 32). In this case, the reactive channel involving a metal type reaction is likely opened up at the higher temperatures of reaction needed to convert *neo*-pentylamine.

Comparison of the product distributions for the three amines shows that a significant amount of condensation products and thiols are found with *n*-pentylamine and *neo*-pentylamine. Thus, substitution is an important pathway for these molecules, especially at low temperature. In contrast, no condensation or thiol products occur for the *tert*-pentylamine HDN, indicating that elimination and hydrogenation are the only relevant reactions. In fact, the E1 mechanism is possible on *tert*-pentylamine because of the stability of the carbocation. This point is highlighted by 22% conversion of *tert*-pentylamine in the blank run at 513 K. This was the only significant background reaction noted in this study.

The results of this study are different from the results reported for bulk sulfides by Cattenot et al. (8) because they were taken at high pressure. Hence, we have a greater propensity for hydrogenation in this study, resulting in pentanes as well as pentenes. Interestingly, earlier results for NiMo/Al_2O_3 operating at 2.0 MPa yielded no condensation products (9). In particular, we operate at the same temperature (523 K), and with sulfur, but also find 2,2-dimethylpropane and condensation products in the effluent. This could be due to the presence of liquid solvent or to the nature of the catalysts.

In comparing our results for quinoline HDN to those for the amine conversion we find that MoS_2 is competitive for hydrogenolysis reactions at low temperatures, but has limited capacity for quinoline HDN at higher temperatures. It is possible that the MoS_2 has poor hydrogenation properties at the elevated temperature, or is affected by the presence of the more complicated feedstock. Our results for MoS_2/SiO_2 resembled those of bulk MoS_2 used by Cattenot et al. (7). In particular, both had good activity for *neo*-pentylamine conversion, and had similar product distributions for *n*-pentylamine conversion, including di(*n*-pentyl)amines.

The results for WP were somewhat different. Here, moderate performance at low temperature for hydrogenolysis was contrasted by good performance at high temperature for both hydrogenation and hydrogenolysis. Thus, The WP catalyst was able to provide a balance of HDN functionalities, including elimination, condensation, and aromatic hydrogenation, which allowed it to survive the shift to higher operating temperature and greater aromatics content. However, compared to the bulk WP sample, the SiO_2

supported WP sample seems to be less capable of hydrogenolysis, as shown by the large amount of hydrogenated products in the effluent (Table 5.4).

The presence of acid sites alone does not lead to active hydroprocessing catalysts, as demonstrated by the inactivity of alumina and silica-alumina supports, acting alone, in hydrodenitrogenation reactions of aromatic heterocycles (20, 33, 34, 35). It is relevant, though, that alumina has been reported as a catalyst for denitrogenation reactions of aliphatic amines leading to olefins, including amines and piperidine (35, 36). The authors of the study on alklamine HDN over the alumina catalyst (36) found that methyl substitution at the α carbon increased the amine reaction rate, while methyl substitution at the β carbon decreased the rate. This is in complete agreement with our findings. Thus, acid-base chemistry alone can explain the results for aliphatic amines.

The origin of the need for hydrogenation activity is related to the requirement of saturation of both the α and β carbon atoms in order to allow the C-N hydrogenolysis reaction to take place. It was on this basis that Nelson and Levy (6) proposed that an E2 mechanism is responsible for the C-N bond cleavage reaction. Thus the activity of catalysts toward aromatic molecules in real feedstocks, such as quinolines, is limited by the ability of the catalyst for hydrogenation of the C_6 ring. Our results confirm independently that C-N bond cleavage is dominated by E2 elimination. Furthermore, our interpretation of results in conjuction with acid-base chemistry is in substantial agreement with the suggestion of Tops□ et al. that the active centers of hydrodenitrogenation catalysts involve Brønsted acid sites (37).

It has been found in the literature that MoS_2 is active for hydrogenolysis reactions, while is not as active for hydrogenation reactions. Our finding that MoS_2/SiO_2 was active for C-N bond hydrogenolysis reactions, but was inactive for quinoline HDN seem to support this established conclusion.

As seen in schemes 5.2 and 5.3, our picture of the catalyst involves an amphoteric surface in which HDN elimination reactions operate by a push-pull mechanism. The amine is pictured adsorbing by hydrogen bonding to a sulfhydril Br□sted acid site. A nearby bridging sulfide group provides the basic site necessary for elimination reaction. The bridging sulfide can be viewed as the conjugate base of the sulfhydril acid site. The sulfhydril site, as pictured, is intimately associated with a coordinatively unsaturated site. Thus measurements of unsaturated sites by CO and O_2 uptake correlate indirectly to the active acid-base sites, but are effective nonetheless.

It has been suggested in the literature that the essential competing reaction for E2 elimination of amines involves nucleophilic substitution of sulfur upon amine groups (7, 8, 9, 38). The resulting thiol is then reported to react quickly by direct hydrogenolysis with hydrogen, forming H_2S and a saturated hydrocarbon. However, this does not properly explain the case of aliphatic thiol decomposition on MoS_2, in which 83% of the product of desulfurization of *n*-butanethiol was found to be olefinic, and butadiene was a major product in the decomposition of tetrahydrothiophene (39). Thus, it is likely that thiols also decompose primarily by E2 elimination, similar to the case for aliphatic amines.

In the case of benzylamine or isoquinoline HDN reactions reported in the literature, HDN proceeds without prior hydrogenation of the C6 ring, but is slower (occurs at higher

temperature) than in the case of aliphatic amines. This suggests that an alternate mechanism, such as one of the metal mediated routes (metal alkyl, aziridinium ring), is available for HDN in cases where the β-carbon is not fully saturated (5, 43). This is verified by the production of hydrocarbons from *neo*-pentylamine found in this study. Thus these metal mediated routes are possible, but the condensation and elimination reactions are easier and thus dominate the reaction pathways of most molecules.

5.5. Conclusions

MoP and WP were prepared on a silica support. They were moderately active catalysts for hydrodenitrogenation of quinoline in a complex mixture. Conversion of a series of amines with different structure confirmed the predominance of the E2 mechanism in the conversion of primary amines to hydrocarbons on these catalysts. The reaction involved formation of adsorbed alkylammonium species and reorganization of bonds by a push-pull mechanism involving acid and nucleophilic species on the surface.

References

1. Li, W., Dhandapani, B., and Oyama, S.T., Molybdenum phosphide: A novel catalyst for hydrodenitrogenation *Chem. Lett.* 207 (1998).
2. Stinner, C., Prins, R., and Weber, Th., Formation, structure, and HDN activity of unsupported molybdenum phosphide *J. Catal.* **191**, 438 (2000).
3. Clark, P., and Oyama, S. T., Synthesis and activity of a new catalyst for hydroprocessing: tungsten phosphide *J. Catal.*, submitted (2000).
4. van Veen, J. A. R., and de Beer, V. H. J., Phosphorus promotion of Ni(Co)-containing Mo-free catalysts in quinoline hydrodenitrogenation *J. Catal.* **161**, 539 (1996).
5. Prins, R., Jian, M., Flechsenhar, M., Mechanism and kinetics of hydrodenitrogenation *Polyhedron* **16**(18), 3235 (1997).
6. Nelson, N., and Levy, R. B., *J. Catal.* **58**, 485 (1979).
7. Cattenot, M., Portefaix, J.L., Afonso, J., Breysse, M., Lacroix, M., and Perot, G., Mechanism of carbon-nitrogen bond scission on unsupported transition metal sulfides *J. Catal.* **173,** 366 (1998).
8. Portefaix, J.L., Cattenot, M., Guerriche, M., and Breysse M., Mechanism of carbon-nitrogen bond cleavage during amylamine hydrodenitrogenation over a sulphided $NiMo/Al_2O_3$ catalyst *Catal. Lett.* **9**, 127 (1991).
9. Portefaix, J. L., Cattenot, M., Guerriche, M., Thivolle-Cazat, and Breysse, M., Conversion of saturated cyclic and noncyclic amines over a sulphided $NiMo/Al_2O_3$ catalyst : mechanisms of carbon – nitrogen bond cleavage *Catal. Today* **10**, 473 (1991).
10. Laine, R. M., *Cat. Rev. -Sci. Eng.* **25**, 459 (1983).
11. Breysse, M., Portefaix, J.L., and Vrinat, M., Support effects in hydrotreating catalysts *Catal. Today* **10**, 489 (1991).
12. Luck, F., *Bull. Soc. Chim. Belges* **100** (11-12), 781 (1991).
13. Marzari, J. A., Rajagopal, S., and Miranda, R., *J. Catal* **156**, 255 (1995).
14. "Cab-o-sil® Untreated Fumed Silica Properties and Functions" Cabot Corporation, Tuscola, IL 1993.
15. Hadden, S. T., and Grayson, H. G., *Hydrocarbon Proc. and Petrol. Refiner* **40**, 207 (1961).
16. Massoth, F. E., and Kim, S. C., Polymer formation during the HDN of indole *Catal. Lett.* **57**, 129 (1999).
17. Oyama, S. T., Schlatter, J. C., Metcalf, J. E., III, and Lambert, J. M., Jr., *Ind. Eng. Chem. Res.* **27**, 1648 (1988).
18. Rundqvist, S., and Lundstrom, T., *Acta Chem. Scand.* **17**, 37 (1963).
19. Rundqvist, S., *Acta Chem. Scand.* **16**(2), 287 (1962).
20. Kraus, H., and Prins, R., *J. Catal.* **170**, 20 (1997).
21. Lopez Cordero, R., Esquivel, N., Lazaro, J., Fierro, J. L. G., and Lopez Agudo, A., *Appl. Catal.* **48**, 341 (1989).
22. Clark, P., and Oyama, S. T., *J. Catal.* submitted, (2000).
23. Katzer, J. R., and Sivasubramanian, R., *Catal. Rev.-Sci. Eng.* **20**, 155 (1979).
24. Siddhan, S., and Narayanan, N., Dehydration of alcohols over oxide catalysts: γ-eliminations - stereospecificity and selectivity *J. Catal.* **59,** 405 (1979).
25. Grimblot, J., *Catal. Today* **41**, 111 (1998).
26. Stumbo, A. M., Grange, P., Delmon, B., *Stud. Surf. Sci. Catal.* **106**, 225 (1997).
27. Weller, K. J., Fox, P. A., Gray, S. D., and Wigley, D. E., Homogeneous models for HDN catalysis *Polyhedron* **16**(18), 3139 (1997).
28. Startsev, A. N., *J. Mol. Catal. A* **152**, 1 (2000).
29. Paul, J., Akpati, H., Nordlander, P., Oh, W. S., Goodman, D. W., and Demirel, B. *Stud. Surf. Sci. Catal.* **106**, 303 (1997).
30. Sonnemans, J., and Mars, P., The mechanism of pyridine hydrogenolysis on molybdenum-containing catalysts: III. Cracking, hydrocracking, dehydrogenation, and disproportionation of pentylamine *J. Catal.* **34,** 215 (1974).
31. Lee, J. H., Hamrin, C. E., Jr., and Davis B. H., Deamination of 2-octylamine with metal nitride and oxide catalysts *Appl. Catal. A* **111,** 11 (1994).

32. Brey, W.S., Jr., and D.S. Cobbledick Catalytic reactions of butylamines over alumina *Ind. Eng. Chem.* **51**(9), 1031 (1959).
33. Menon, R., Joo, H. S., Guin, J. A., Reucroft, P. J., and Kim, J. Y., *Energy and Fuels* **10**, 579 (1996).
34. Reinhoudt, H. R., Troost, R., van Schalkwijk, S., van Langeveld, A. D., Sie, S. T., Schulz, H., Chadwick, D., Cambra, J., de Beer, V. H. J., van Veen, J. A. R., Fierro, J. L. G., and Moulijn, J. A., Application of ASA supported nobel metal catalysts in the deep hydrodesulphurization of diesel fuel *Stud. Surf. Sci. Catal.* **106**, 237 (1997).
35. Ledoux, M. J., Bouassida, A., and Benazouz, R., The use of pyridine and piperidine HDN as probe for activity of molybdenum-based hydrotreatment catalysts. The role of nickel (part II) *Appl. Catal.* **9**, 41 (1984).
36. Hogan, P., and Pasek, J., Reaction of amines on acid catalysts. IV. Kinetics and mechanism of olefin formation from triethylamine and diisopropylamine on γ-alumina *Coll. Czech. Chem. Comm.* **38**, 1513 (1973).
37. Tops□, N. Y., Topsøe, H., and Massoth, F. E., *J. Catal.* **119**, 252 (1989).
38. Vivier, L., Dominguez, V., Perot, G., and Kasztelan, S., Mechanism of C-N bond scission. Hydrodenitrogenation of 1,2,3,4-tetrahydroquinoline and of 1,2,3,4-tetrahydroisoquinoline *J. Mol. Catal.* **67**, 267 (1991).
39. Kolboe, S., Catalytic hydrodesulfurization of thiophene. VII. Comparison between thiophene, tetrahydrothiophene, and *n*-butanethiol *Can. J. Chem.* **47**, 352 (1969).